ACS Energy LETTERS

http://pubs.acs.org/journal/aelccp

Semitransparent Perovskite Solar Cells

Stav Rahmany and Lioz Etgar*

Cite This: *ACS Energy Lett.* 2020, 5, 1519−1531

Read Online

ACCESS | Metrics & More | Article Recommendations

ABSTRACT: Solar cells are one of the most attractive nonpolluting energy sources. In this field, hybrid and inorganic perovskite, which is a semiconductor, has been shown to function efficiently in solar cells. One of the unique properties of perovskite allows it to become semitransparent, and not just by controlling its optical properties. In this Focus Review we provide the most updated methods and techniques to make semitransparent perovskite solar cells: (i) the use of thin perovskite film; (ii) the possibility to self-assemble the perovskite on a photoanode, providing an empty transparent area while not sacrificing the light-harvesting efficiency; (iii) the use of solvent properties to form islands of perovskite using dewetting on the surface; and (iv) the possibility to form a transparent contact that makes the solar cell fully semitransparent. Finally, the potential and future features of semitransparent perovskite solar cells are presented.

In recent years, perovskite-based solar cells have remarkably increased their power conversion efficiency (PCE), achieving values greater than 25%.[1] Therefore, perovskite solar cells are considered as an excellent candidate to replace the common, Si-based solar cells that currently dominate the photovoltaic (PV) market. Perovskite has a chemical formula of ABX_3, where A is a monovalent cation (e.g., methylammunium, formammidinium, or Cs), B a divalent rare metal (Pb^- or Sn^-), and X a halide anion (I^-, Br^-, or Cl^-).[2−6] Perovskite has unique optical and electrical properties, such as a high absorption coefficient,[7,8] a long charge carrier diffusion length,[9,10] and a direct and tunable band gap.[11,12] Among these advantages, the perovskite fabrication process is based on a solution process that enables a variety of relatively easy deposition techniques, such as spin coating, screen printing, and evaporation.[13−16] Because of the attractive properties of perovskite (mainly band gap tuning and different solar cell architectures), it is possible to fabricate semitransparent solar cells where part of the light can pass through the cells and some of it is absorbed by the light-harvesting layer. The transparency can be achieved either by making a thin perovskite layer or by partial coverage of the perovskite, which leaves areas of the transparent substrate empty. In addition, by tuning the band gap, it is possible to control the transparency as well.

Semitransparent solar cells can function as windows in buildings and skyscrapers, providing both shading and green electricity to the building. In 2018 the residential and commercial sectors accounted for about 40% (about 40 quadrillion BTU) of the total U.S. energy consumption, whereas renewable energy sources accounted for about 11% of the total U.S. energy consumption and about 17% of the electricity generated.[17,18] Building integrated photovoltaic (BIPV) systems can significantly reduce the building energy consumption and greenhouse gas emission by producing electricity without any dependence on the electrical grid. In addition, most conventional solar cells are mainly located on rooftops or in open areas in order to achieve maximum exposure to sunlight where the semitransparent solar cells can be integrated into the sides of the building and can maximize the space capacity and therefore the energy production.

In this work we discuss several possible options to achieve semitransparent perovskite-based solar cells. This Focus Review is divided into five parts (thin films, dewetting, self-assembly, transparent back contact and tandem applications); it discusses how semitransparency in perovskite-based cells can be achieved and the connection between transparency and the photovoltaic parameters.

Semitransparency Using Perovskite Thin Films. The band gap of perovskite is dictated mainly by the halides (bromide, iodide, and chloride). As the halide radii decrease, the perovskite band gap increases, enabling more light in the visible region to pass through the perovskite film.[19] Therefore, it is possible to change the transparency of the perovskite layer

Received: February 23, 2020
Accepted: April 6, 2020
Published: April 6, 2020

https://dx.doi.org/10.1021/acsenergylett.0c00417

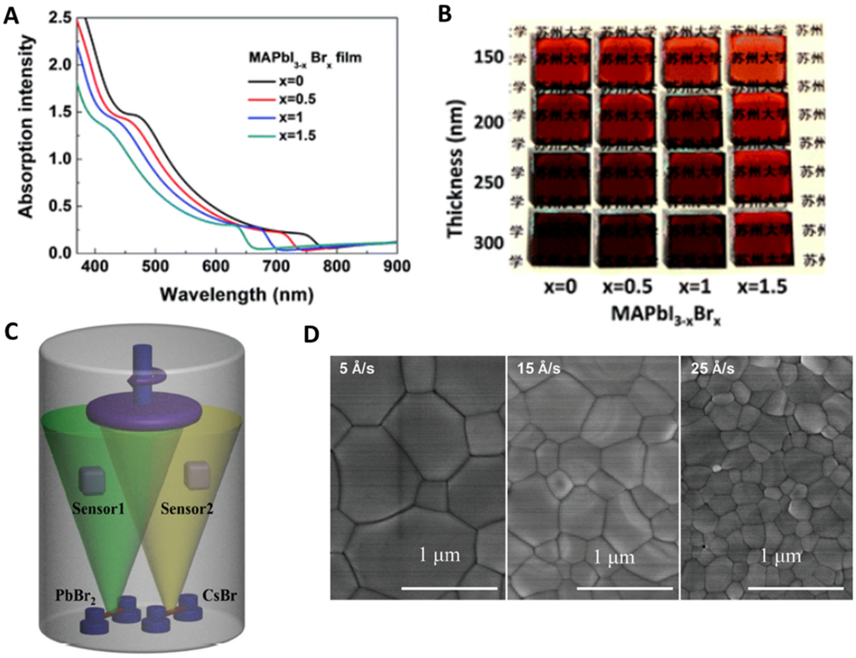

Figure 1. (A) Absorbance spectrum of $MAPb(I_{3-x}Br_x)_3$ for different x values (i.e., Br content). (B) Transmittance changes as a function of the amount of Br and the perovskite thickness. (C) Schematic illustration of the dual source deposition of $CsPbBr_3$ and (D) the grain size as a function of the evaporation rate. Reprinted with permission from refs 20 and 23. Copyright 2018 John Wiley and Sons and 2013 Royal Society of Chemistry, respectively.

by changing the bromide-to-iodide ratio in the perovskite, where $MAPb(I_{3-x}Br_x)_3$ ($0 \leq x \leq 3$). If there is a constant thickness of the perovskite film, the average transparency (AVT) of the film increases as the bromide ratio becomes higher, varying from 10% AVT when $x = 0$ to 24% AVT when $x = 1.5$ if there is 300 nm film thickness.[20] As shown in Figure 1A, incorporating more bromide shifts the absorbance spectra to the blue because of an increase in the band gap; this leads to spectral losses and to a decrease in the power conversion efficiency (PCE) of the cell. On the other hand, it has been shown that more bromide in the perovskite lattice improves the crystallinity and consequently improves the photovoltaic activity.[21]

Another approach to achieve semitransparency[14] is to maintain the amount of bromide (or iodide) constant while changing the film thickness by varying the solution concentration. In order to achieve maximum absorbance, a perovskite film thickness of 400 nm is required.[22] A thinner film of perovskite will enable some of the light to pass through, based on its absorption coefficient, which depends on the wavelength. Figure 1B shows different thicknesses (150, 200, 250, and 300 nm) for each x value; it is clear that the AVT of the cell is reduced as the film becomes thicker.

As described above, the most common method to achieve semitransparent perovskite solar cells is by reducing the film thickness using a low concentration of the perovskite solution. The main difficulty in using this method is the need to form a uniform and pinhole-free film when the film thickness is very thin. To overcome this problem, it is possible to deposit the perovskite by an evaporation technique. Li et al. fabricated a thin layer of $CsPbBr_3$ by a dual-source vacuum coevaporation (DSVE) method for planar architecture devices.[23] Usually $CsPbBr_3$ is fabricated via a two-step deposition method by spin coating, because the reaction between CsBr and $PbBr_2$ is incomplete and pinholes can be formed.[24] As seen in Figure 1C, in DSVE both precursors (CsBr and $PbBr_2$) are evaporated simultaneously and are then annealed to obtain a single-phase perovskite film where the evaporation rate enables one to control the crystallinity, grain size, and film thickness. As shown in Figure 1d, the grain size increases when the evaporation rate is slower, which minimizes the grain boundaries. Moreover, no pinholes are observed in these evaporated films. Because this perovskite composition does not absorb light through the entire visible region, the semitransparent $CsPbBr_3$-based solar cells can achieve an AVT of nearly 60% in the wavelength range of 530−800 nm and a PCE of 5.98%.

The problem of surface coverage for a thin-film layer of perovskite becomes more significant in the planar-based perovskite solar cell architectures. Unlike mesoporous layers, the surface area of the planar film is more limited than that of the mesoporous film;[25] therefore, the fabrication of thin layers in the planar perovskite solar cell architecture becomes more challenging in terms of continuous and uniform perovskite film. To overcome this problem, Bag et al. introduced a surface passivation treatment for the PEDOT:PSS film using thiourea vapor at different time lengths, as described in Figure 2A.[26] The interaction between Pb and I is improved because of the passivation of the PEDOT:PSS film by chalcogenide species; therefore, the surface coverage is better. The perovskite deposition was made by a two-step process, whereby the PbI_2 layer dictates the final thickness of the perovskite layer. As shown in Figure 2B, different thicknesses of perovskite were fabricated from 65 nm film, which was more transparent than the 310 nm film. This technique enables the formation of a uniform, pinhole-free, 110 nm perovskite film with an AVT of 34% and a PCE of 8.2%.

The transparency of the perovskite film can also be adjusted by the solvent type, which affects the formation of the intermediates of the perovskite and the solvent. The most

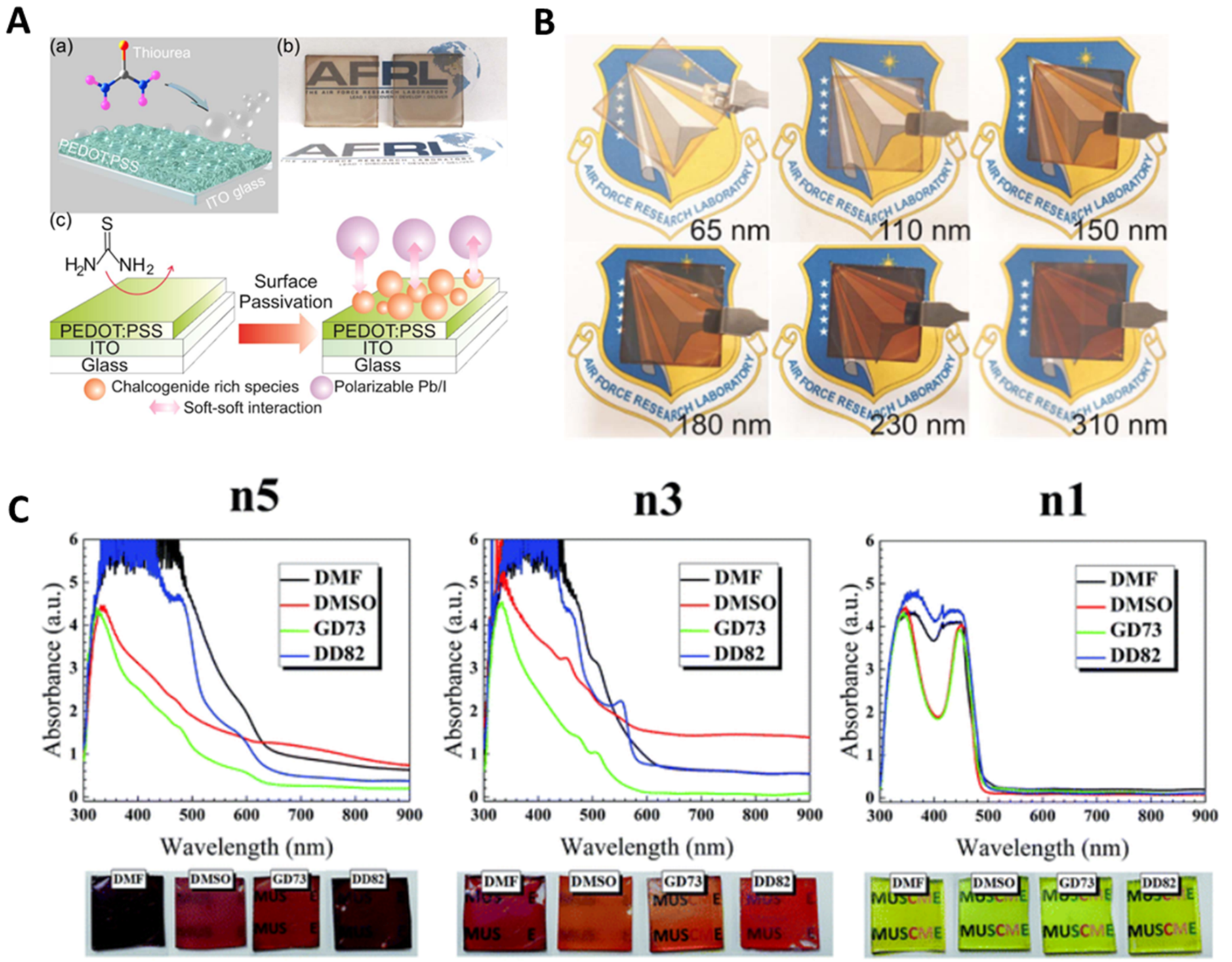

Figure 2. (A) Passivation treatment process of PEDOT:PSS using thiourea and (B) different thicknesses of perovskite film on top of the treated layer. (C) Absorbance spectrum for $(PEA)_2(MA)_{n-1}Pb_nI_{n+1}Br_{2n}$ at different n values using different solvents. Images of the film are shown for each condition. Reprinted with permission from refs 26 and29. Copyright 2016 Elsevier and 2019 Royal Society of Chemistry.

common solvents for the perovskite solution are DMSO, DMF, NMP, and GBL, or a mixture of them.[27,28] Ponchai et al. used a low-dimensional perovskite having the composition $(PEA)_2(MA)_{n-1}Pb_nI_{n+1}Br_{2n}$ in three different systems of $n = 1$, 3, and 5, where each n value gives a different band gap for semitransparent applications.[29] The authors studied the effect of solvent type and solvent mixing on the 2D perovskite composition. The graphs in Figure 2C show the change in the absorption edge as a function of the n value and the solvent type. There is a blue shift in the absorbance spectrum as the n value decreases, because of quantum confinement. The pictures in Figure 2C show the change in color when different solvents are used for the same n value; when $n = 5$ and 3, it can be seen that the solvent affects the transparency of the film, whereas when $n = 1$ the impact of the solvent type is minor because of the lack of a small cation at the A site. Another factor that affects the absorption is the solvent type. A high boiling point solvent will evaporate slower than a low boiling point solvent; hence, it will form a thinner film. DMF and a mixture of DMF/DMSO produced darker films having a higher absorption. In contrast, intermediate phases are formed with DMSO, which impedes the crystallization rate; therefore, some bright areas appear in the film. The viscosity of the solvent also affects the crystallinity, and therefore, it will change the absorbance. Large grains and uniform morphology can be achieved with a low-viscous solvent because of easier diffusion and the interactions of the molecules and the nuclei. Overall, having a mixture of DMF:DMSO (at a ratio of 8:2) resulted in the best balance between solvents that produce a good surface morphology, large crystal size, and have few defects, along with a semitransparent perovskite film.

Self-Assembly of Perovskite Resulting in Semitransparency. The fact that perovskite is a solution-based process makes it possible to form it by self-assembly using a wet-deposition method.[30,31] Aharon et al. demonstrated that a perovskite grid structure pattern can be formed by using mesh-assisted deposition under ambient conditions.[32] As shown in Figure 3A, the perovskite is deposited on top of mesoporous TiO_2, and by the self-assembly process, the material crystallizes along the mesh wires, forming the perovskite grid pattern. The grid pattern provides empty areas through which the light can pass; this produces a semitransparent solar cell, as shown in Figure 3B. The main advantage of this self-assembly process is that there is no need to compensate for the perovskite film thickness, unlike thin-film semitransparent perovskite solar cells (SPSCs) in which the perovskite film thickness is below

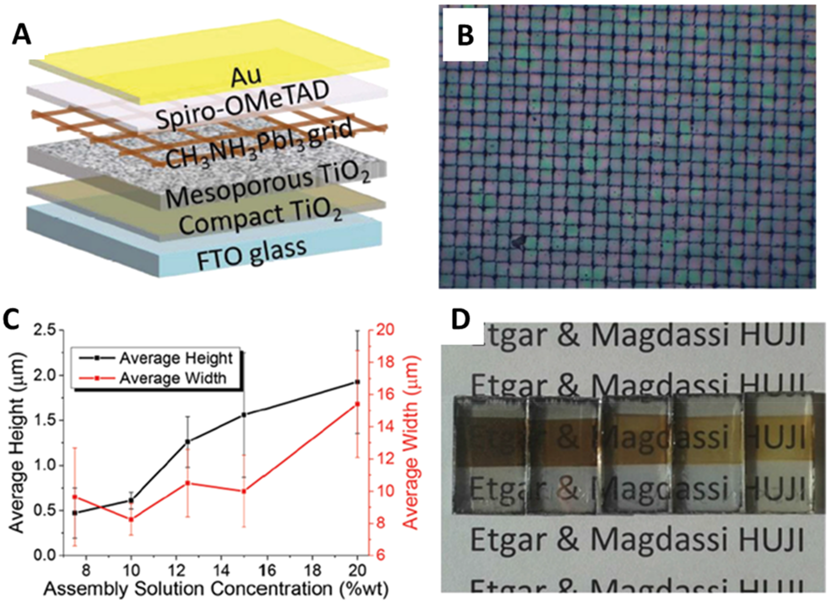

Figure 3. (A) Schematic illustration of the perovskite grid cell structure. (B) Optical microscopy image of the perovskite grid pattern. The light can pass through the TiO_2-exposed areas. (C) Grid average height and width as a function of the perovskite solution concentration. (D) Images of the perovskite films that were made with different concentrations from 20% (left film) to 7.5% (right film). Reprinted with permission from ref 32. Copyright 2015 John Wiley and Sons.

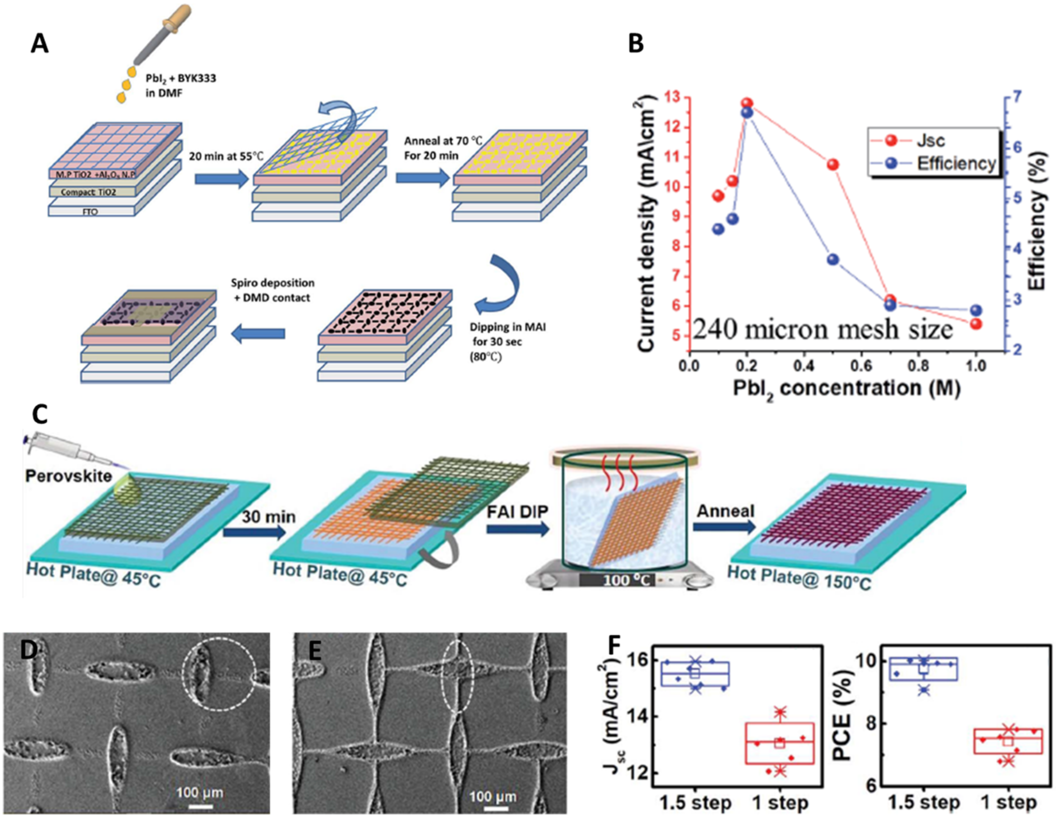

Figure 4. (A) Schematic illustration of the grid deposition via the two-step method. (B) Effect of the PbI_2 concentration on the current density and the PCE of the grid cells fabricated by two-step deposition. (C) Schematic illustration of the FAI postdeposition treatment and SEM images that show the difference in the grid pattern between (D) nontreated and (E) FAI-treated grids. (F) Comparison of the current density and the PCE of treated and nontreated devices. Reprinted with permission from refs 35 and 39. Copyright 2016 and 2013 Royal Society of Chemistry.

the maximum absorbance thickness.[33,34] Two main parameters can control the semitransparency of the device: (1) the size of the mesh openings (when the openings are large, more light will pass through) and (2) the perovskite concentration, which affects the width of the grid walls and their height. Figure 3C shows the tendency of the grid width and height with the perovskite concentration. Figure 3D shows the changes in the transparency of the perovskite layer as a function of the solution concentration, where the transmittance decreases as the concentration becomes higher. This unique architecture exhibited 20−70% transmittance along with a PCE of 0.4−5%, respectively.

Further improvement in this self-assembly process was achieved by Rahmany et al., who formed a perovskite grid using a two-step deposition method on top of ETL composed of mesoporous TiO_2 and Al_2O_3 NPs.[35] As shown in Figure 4A, in the first step, a grid of PbI_2 is formed by the mesh-assisted deposition method when different concentrations of the solution were studied. After the solvent is evaporated, the PbI_2 grid is dipped in the organic cation ($CH_3NH_3^+$) to form the desirable $MAPbI_3$ grid. In this way, the surface coverage and perovskite crystallinity improve. It appears that the use of a relatively high PbI_2 concentration (>0.5M) significantly reduces the AVT, because more material covers the surface. Figure 4B shows that the best PCE is achieved for 0.2 M PbI_2 and that above this concentration, both current density and PCE dropped. The decrease in the photovoltaic parameters is due to incomplete conversion of the perovskite to the black phase and to PbI_2 residues. The optimal PbI_2 concentration exhibits a PCE of ~8% with gold as a back contact and an AVT of ~25% for the active layer. To make a complete semitransparent device, a transparent dielectric metal dielectric (DMD) back contact, which was composed from MoO_3/Au/MoO_3, was thermally evaporated to afford a PCE of 5.5% with over 20% transmittance for the complete device.

Additional improvement of this structure was reported by Rai et al., who applied a mixed cation perovskite,[36−38] $Cs_{0.2}FA_{0.8}Pb(I_{0.6}Br_{0.4})_3$, together with an additional half step of dipping the perovskite film in hot FAI solution.[39] Figure 4C shows the grid formation process and the postdeposition treatment. At the beginning, a grid of the mixed-cation mixed-halide is formed by the mesh-assisted deposition and annealed. After the solvent residues are removed, the perovskite grid is dipped in a hot FAI solution for 40 s. Because the grid deposition method is based on self-assembly in which the solvent evaporates slowly, the crystallinity of the perovskite film is incomplete. The hot FAI in isopropanol (IPA) solution provides mobile ions that assist in the conversion of the unreacted iodide and bromide perovskite phases. In addition, the nontreated perovskite exhibits an incomplete formation of the grid pattern, whereas after the treatment, the grid becomes intact, as shown in panels D and E of Figure 4, respectively. As a result of the postdeposition treatment, the AVT slightly decreased from 36% to 28%, whereas the current and PCE improved dramatically (Figure 4F), which yielded a PCE of 10% (with an AVT of more than 20%), compared to 8% in the treated and nontreated devices, respectively. Furthermore, the treated cells exhibit better stability over time, along with improved charge-transfer abilities.

> One of the exciting properties of perovskite is the ability to make it semitransparent and therefore to fabricate a semitransparent perovskite solar cell.

The Dewetting Process Produces a Semitransparent Perovskite Layer. The dewetting process is based on the slow evaporation rate of the solvent. By highly controlling the evaporation rate, it is possible to create a semitransparent perovskite film.[40,41] Eperon et al. reported on the fabrication of microstructures of perovskite ($FAPbI_3$ or $MAPbI_3$) islands by using an excess of organic material in the precursor solution, together with a low-vapor-pressure solvent (DMSO).[42,43] Figure 5A shows a schematic illustration of the cell structure; the deposition was performed on top of compact TiO_2, forming a planar architecture perovskite solar cell using two types of perovskites with a different A site cation (MA^+ or FA^+). As a result of the solvent type, the perovskite crystallization occurs slowly while the solvent is still present, which leads to the formation of discontinuous perovskite islands, as can be seen in the SEM image in Figure 5B. The synthesis of the $FAPbI_3$ perovskite

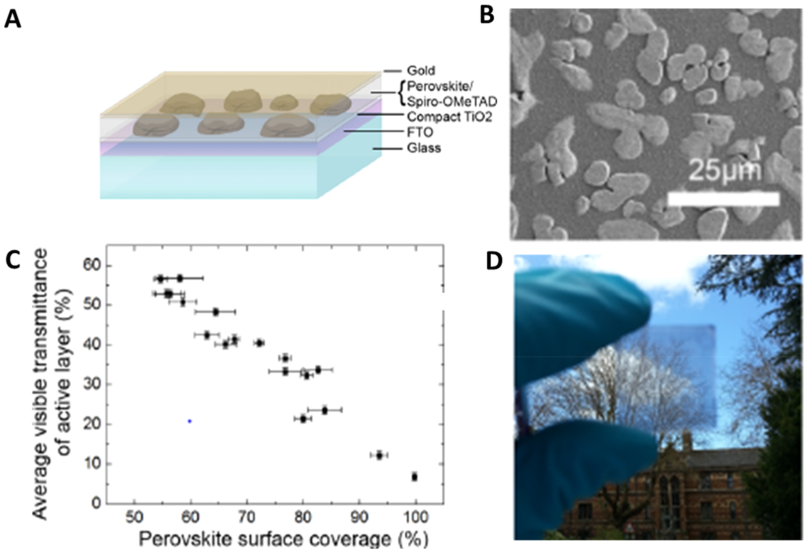

Figure 5. (A) Schematic illustration of the microstructural perovskite islands on top of compact TiO_2. (B) SEM image of the perovskite islands after the dewetting process. (C) Transmittance of the active layer as a function of the surface coverage. (D) Image of the neutral color semitransparent perovskite. Reprinted with permission from refs 42 and 43. Copyright 2015 and 2014 American Chemical Society.

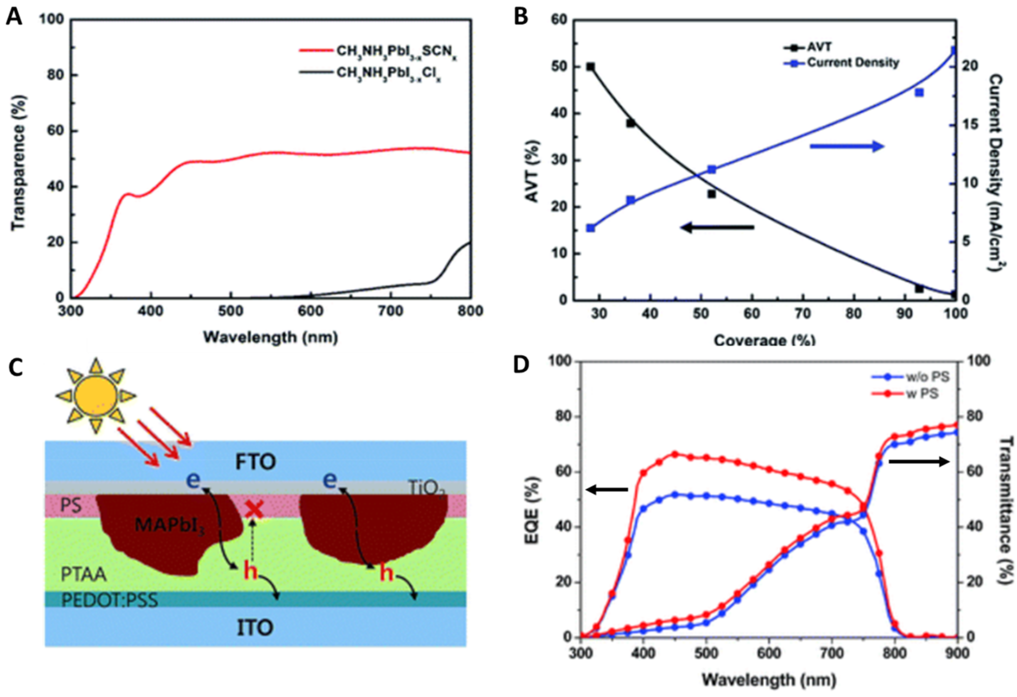

Figure 6. (A) Effect of SCN on the transmittance of the perovskite layer and (B) the AVT and current density of the SCN perovskite as a function of the surface coverage. (C) Schematic illustration of the cell structure with the PS layer. The PS covers only the substrate areas and prevents direct contact between the TiO_2 and PTAA. (D) EQE and transmittance of the device with (red) and without (blue) PS. Reprinted with permission from refs 44 and 50. Copyright 2017 and 2016 Royal Society of Chemistry.

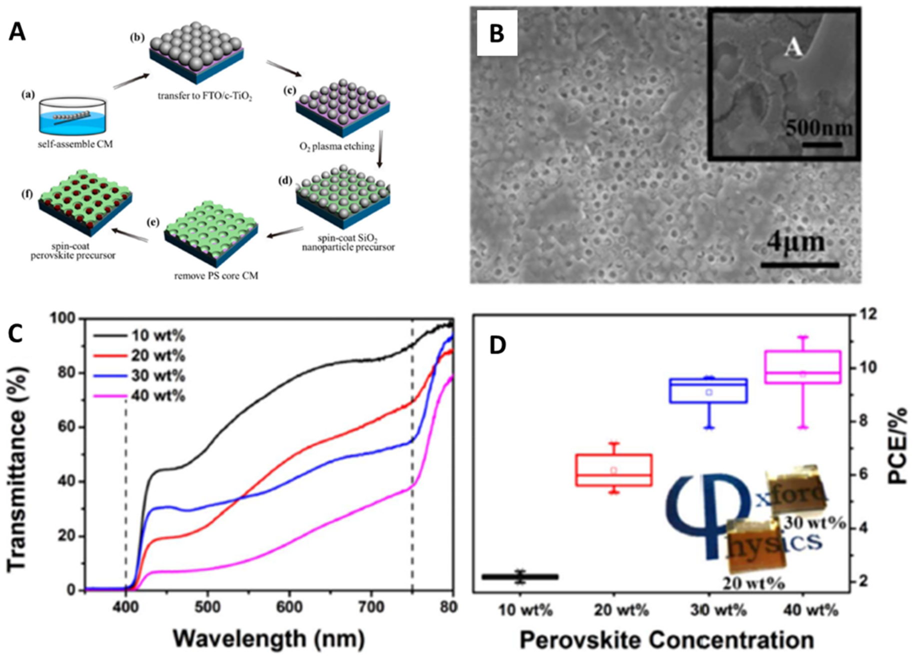

Figure 7. (A) Illustration of the SiO_2 honeycomb formation process and (B) SEM image of the architecture filled with perovskite. (C) Transmittance and (D) PCE of the honeycomb semitransparent cells as a function of perovskite concentration. Reprinted with permission from ref 51. Copyright 2017 Elsevier.

includes the precursors MAI, FAI, and $PbCl_2$, which react based on the following reaction:

$$2MAI + FAI + PbCl_2 \rightarrow FAPbI_3 + 2MACl$$

The same perovskite microstructure architectures can be formed with $MAPbI_3$ by a similar reaction:

$$3MAI + PbCl_2 \rightarrow MAPbI_3$$

The transmittance of the perovskite film is dictated by the surface coverage, which can be controlled by different processing conditions. As indicated in Figure 5C, the surface coverage ranges from 55% to 100%, when the transmittance of the active layer decreases and as the coverage percentage increases. This method does not require reducing the

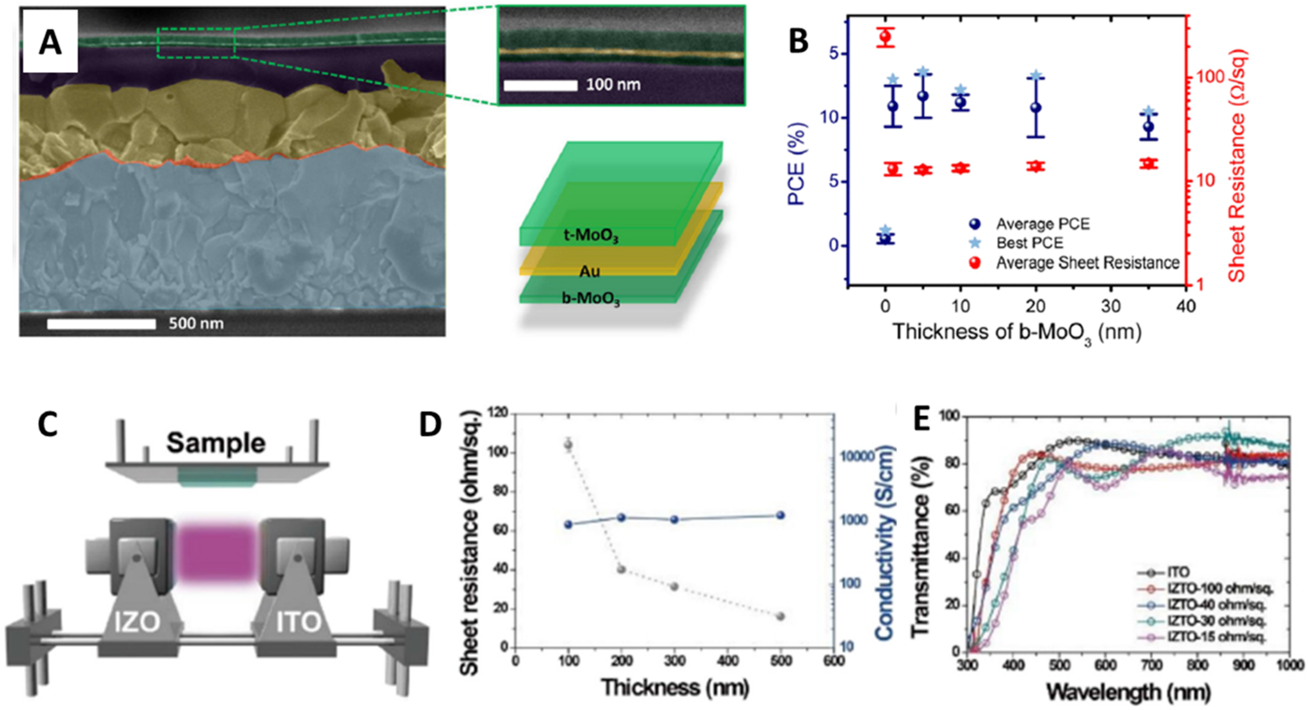

Figure 8. (A) Cross section of an SEM image of the semitransparent solar cell. The inset shows the DMD contact as illustrated in the attached scheme. (B) PCE and sheet resistance as a function of the MoO_3 bottom layer thickness. (C) Illustration of the linear facing target spattering method for IZTO contact. (D) Sheet resistance and conductivity as a function of the IZTO electrode thickness and (E) the transmittance of electrodes with different thicknesses. Reprinted with permission from refs 54 and 61. Copyright 2015 and 2019 Elsevier.

perovskite film thickness (the same as in the case of the self-assembly method), because the light passes through the exposed areas where there is only TiO_2. These cells exhibit a neutral color, as shown in Figure 5D. The FA-based perovskite displayed higher solar cell performance and smaller hysteresis than did the MA-based solar cells, with an efficiency of 6.4% and with an AVT of 34%.

Chen et al. used a novel strategy using $Pb(SCN)_2$ as the lead source, together with an excess of CH_3NH_3I to fabricate $CH_3NH_3PbI_3$ microstructural islands for semitransparent cells.[44] Here, the authors reported that the perovskite islands formed immediately after the spin coating, without any need for annealing in order to remove an excess of the organic part. Because the $Pb(SCN)_2$ concentration in the precursor solution is high, the surface coverage is reduced, enabling more light to pass through the cell; therefore, it increases the transmittance without reducing the crystallinity of the perovskite. As shown in Figure 6A, the highest $Pb(SCN)_2$ ratio increases the transparency from 1.3% to 50%, yielding a PCE of 2.4%. Figure 6B demonstrates the trade-off between the AVT and the current density as a function of the surface coverage, because the surface coverage decreases the AVT increase because of less material on the surface and enhancement of the substrate-exposed areas. On the other hand, in addition to the fact that less active material is present, the exposed areas are potential recombination centers because of a direct contact between the ETL and the HTL in those areas.

Most of the perovskite solar cell structures have a hole-conductor layer.[45−47] Because partial coverage deposition methods leave exposed areas on the substrate (mostly in the case of electron transport layers), the light can go through these empty areas, creating semitransparency; however, this forms a direct contact between the ETL and the HTL, which enhances recombination.[48,49] To overcome this problem, Im et al. used spin coating and spin washing of polystyrene (PS), which fill only the exposed areas without covering the perovskite's islands.[50] The schematic illustration in Figure 6C shows the cell structure and the coverage of the exposed areas by PS; this coverage prevents direct contact between the ETL and HTL. Figure 6D shows the enhancement in the EQE of a device with PS (red), compared to a device without PS (blue), whereas the transmittance remains the same. The coverage of the empty areas leads to an increase in the photovoltaic parameters of the semitransparent solar cell (with a J_{sc} value of 15.5 mA/cm^2, a V_{oc} value of 0.96 mV, and a fill factor of 71% with PS, compared to 12.3 mA/cm^2, 0.87 mV, and 61.7% without it), resulting in a PCE of 10.6%, along with an AVT of ~20.9%.

Another way to control the surface coverage and perovskite patterning is by designing a scaffold layer for perovskite deposition. Figure 7A shows the layer-by-layer process reported by Snaith et al., where the SiO_2 honeycomb (HC) structure was spin coated over PS nanoparticles, which then were removed by plasma etching.[51] The coverage can be controlled by the PS particles' size and the plasma etching time. After the desired pattern was achieved, different concentrations of perovskite solution were spin coated on top of the HC SiO_2 that occupied the positions of the PS spheres, as shown in Figure 7B. The plasma etching time directly affects the AVT of the active layer. The transmittance increases as the plasma time increases, as a result of increasing the interstitial area between adjacent PS spheres. The perovskite solution concentration also affects the AVT of the active layer. Figure 7C shows the decrease in the transmittance as the perovskite concentration increases. When a low-concentration solution (below 20 wt %) is used, perovskite

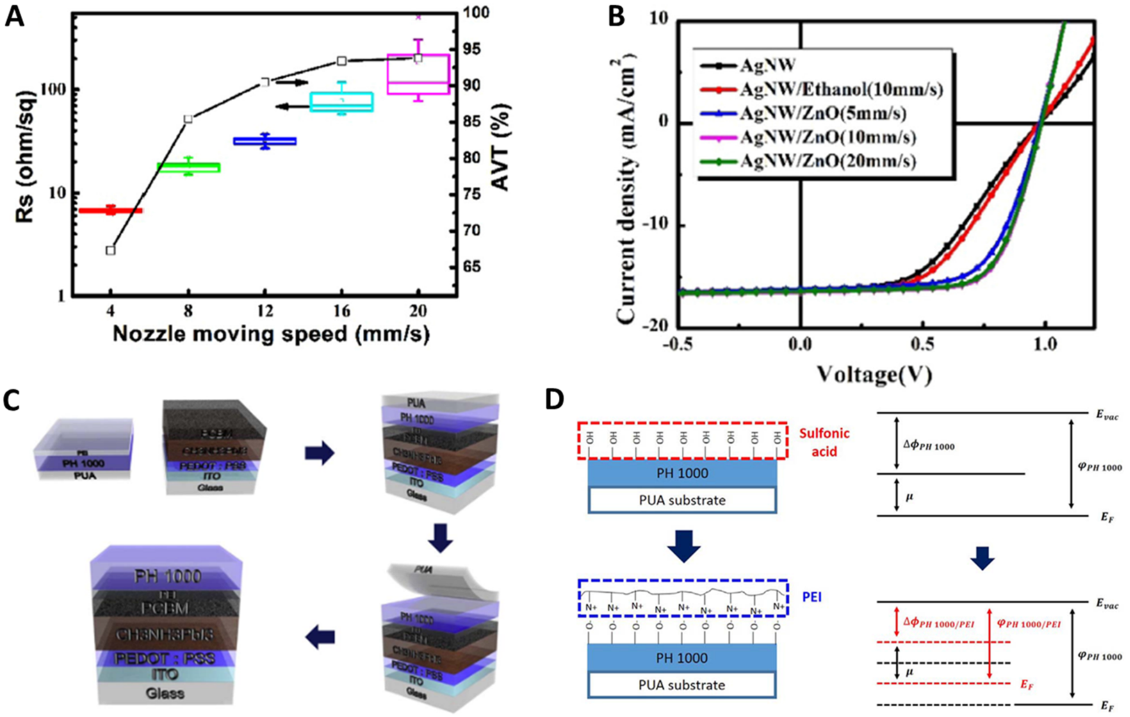

Figure 9. (A) AVT and series resistance (Rs) of the Ag NWs electrode as a function of the nozzle moving speed. (B) *J*−*V* curves of cells with a Ag NWs electrode only and Ag NWs with an overlayer of ZnO nanoparticles that contribute to the enhancement of the fill factor. (C) Polymer stamping process of the PH1000/PEI electrode and (d) the change in the work function as a result of the PEI layer. Reprinted with permission from refs 62 and 64. Copyright 2018 Elsevier.

domains are randomly formed within the HC SiO_2 scaffold, which limits the perovskite growth to pore size. However, higher concentrations will lead to a capping layer on top of the HC structure, because the pores are significantly smaller than the randomly formed perovskite crystals. As the concentration increases, the thickness of the capping layer becomes thicker, which reduces the AVT of the active layer because of a thicker capping layer that contributes to a higher PCE, as shown in the graph in Figure 7D. The best solar cell using this method was fabricated with 30 wt % perovskite solution, where the HC scaffold was formed with 600 nm PS and 8 min of plasma etching; this results in a PCE of 10.3% and an AVT of 38%.

Transparent Contact. Semitransparent perovskite solar cells cannot be completed without a transparent back contact. In most of the perovskite solar cells, including the ones discussed earlier in this Focus Review, the back contact is a relatively thick (~70 nm or more) metal film, which because of a high refractive index, blocks the light from passing through it. In order to make a fully semitransparent perovskite solar cell, a transparent contact is needed. This can be achieved by various techniques and materials, such as 2D structures, transparent conductive oxides (TCOs), metal NWs, graphene electrode, and more.[52,53] In addition, a transparent contact can also be used for a tandem configuration where the light can go through from the bottom cell to the upper cell. One option to achieve a transparent contact is to evaporate a thin metal layer as a back contact that will allow some of the light to pass through. However, this option still has some reflectance issues due to the interface between the metallic layer and the air. Moreover, here there is insufficient coverage of the metal because of the roughness of the layer below it. Cheng et al.[54] demonstrated a dielectric−metal−dielectric (DMD) composition for transparent back contact. The DMD composition, shown in Figure 8A, is composed of a bottom layer of MoO_3, a thin layer of Au, and a top layer of MoO_3. The bottom MoO_3 layer functions as a seeding layer that allows better surface coverage of the thin Au film, enabling the formation of a continuous layer. The top MoO_3 layer protects the reflectance of the metal and defines the transmission window of the DMD structure. As shown in Figure 8B, when a thin Au layer is deposited directly on the HTL, it exhibited high series resistance ($4.3 \times 10^3\ \Omega\ cm^2$); however, when even a very thin MoO_3 bottom layer (1 nm) is deposited on top of the HTL, the conductivity improves significantly (13−15 $\Omega\ cm^2$). On the other hand, a thick bottom MoO_3 layer (20 nm) will reduce the charge extraction from the HTL and will reduce the efficiency. It is also possible to increase the conductivity of the contact by depositing a thicker Au film for better percolation; however, it will reduce the overall transparency of the contact and the cell.

Promising candidates for transparent electrodes are mainly transparent conductive oxides (TCOs). Some examples include indium tin oxide (ITO) and fluorine-doped tin oxide (FTO), which exhibit high conductivity, high transmittance in the visible region, and good reproducibility.[55,50,56−58] Along with those excellent qualities, TCOs are deposited by thermal sputtering, which requires high temperatures (>300 °C) that are likely to damage the HTL, which is mostly an organic compound. One approach to overcome the sputtering damage is by deposit a buffer layer which will protect the layer underneath. Werner et al. introduced transition metal oxide (TMO) of WO_x as a buffer protecting layer on which ITO was sputtered. It was shown that WO_x is more durable to sputtering damage and leads to spectral gains by reducing the sub-band gap parasitic absorption.[59] The same principle can be applied by using other buffer layer materials such as MoO_x or VO_x.[56,60] On the other hand, Na et al.[61] introduced indium zinc tin oxide (IZTO) electrodes grown by linear facing target sputtering (LFTS) without any thermal treatment using a dual source with ITO and IZO, as illustrated in Figure 8C. Unlike other evaporation techniques, in this method the high plasma energy between the target and the substrate position is effectively confined. Figure 8D shows that the sheet resistance of the IZTO can be easily controlled via the thickness of the layer, because as the film gets thicker, the resistance tends to decrease, whereas no significant change in the conductivity was observed because of the completely amorphous structure of the IZTO electrode. The AVT values for the IZTO electrode in the region between 370 and 740 nm were above 70%; there is a slight decrease as the thickness increases (Figure 8E). A perovskite solar cell fabricated with the IZTO electrode exhibited a similar PCE of 12.85%, compared with 13.48% for the Ag-based electrode (non-transparent contact). Overall, a complete semitransparent cell with the IZTO electrode and a perovskite layer exhibited a PCE of 8.3% and an AVT of 33.9%.

An alternative to the evaporation process involving a transparent contact electrode is a solution-based process that makes the deposition easier and reduces the cost. Among the most promising candidates in the field of solution-based materials for semitransparent electrodes are silver nanowires (Ag NWs). The lamination process was demonstrated by Peumans et al.,[62] who fabricated random meshes of metal nanowires that function as transparent top electrodes. These meshes achieved the same sheet resistance and transparency as the metal oxide electrodes. Cui et al.[63] used inkjet printing of Ag NWs on top of a thin polyethylenimine (PEI) protecting layer, which also serves as a work function modifier. The authors also introduced a spray coating deposition of Ag NWs where the layer thickness can be controlled by the nozzle speed, which affects the AVT and sheet resistance of the electrode, as described in Figure 9A. Both parameters decrease, along with the spray coating speed, because of the formation of a denser Ag NW film. To further improve the contact, a top layer of ZnO NPs was sprayed onto the Ag NW. Figure 9B shows the effect of the ZnO NPs on the $J-V$ curve, which mainly improves the fill factor of the cells. The AVT of the composite electrode slightly increased because of the scattering effect of the ZnO NPs, whereas the sheet resistance decreased as the ZnO layer thickness increased, as a result of the improved connection between the layers and consequently better conductivity. Furthermore, the ZnO layer improves the surface coverage and fills the voids in the Ag NWs, which improves the connection between the contact and the underlying layer. A neat Ag NWs electrode yielded a PCE of 13.27% and an AVT of 16.3%, whereas the device with the ZnO NPs overlayer exhibited a PCE of 11.31% and an improved transparency of 23.3%.

> One of the main remaining challenges is the scale-up process of solar cell production, where the goal is to fabricate a semitransparent solar cell that can be used instead of a window.

Stamping transfer is considered as a good alternative process for fabricating transparent contact for perovskite-based solar cells instead of the thermal evaporation technique, because high temperatures are not required. In addition, the process does not involve any solvents like in the case of solution-based techniques, which can harm the other layers in the structure. Wang et al.[64] showed a stamping transfer of PEDOT:PSS (PH 1000)/PEI by using polyurethane acrylate (PUA) as the polymer stamp. Figure 9C shows the polymer stamping process in which PH1000/PEI is first deposited on top of the polymer, and in the next stage, it is stamped onto the top layer of the device. In the final stage, the polymer is removed without damaging the electrode or the underlying layer. In this way, the layers transfer to the device without degrading or damaging the perovskite layer. Figure 9D shows that the PEI layer reduces the work function and the surface dipole of the PEDOT:PSS film and increases the interfacial charge-transporting condition between PH1000 and the ETL. However, the polymer stamping electrode exhibits a poor conductivity of 1.08 × 101 S/cm compared to 3.69 × 105 S/cm for a neat Al contact, which results in a PCE of 4.21% and an AVT of 24.53% for the complete device.

Tandem Applications. The ability to tune the perovskite's band gap makes those solar cells an excellent option to be used in tandem configuration. Tandem solar cells are composed from several single-junction cells with different tailored band gaps that can maximize the light absorption and minimize the spectral losses of the light-harvesting layers. This architecture can increase the PCE by overcoming the theoretical limits of the single-junction solar cell.

The most common tandem configuration involved a crystalline silicon (c-Si) solar cell conjugated with a perovskite cell having a band gap between 1.7 and 1.8 eV. Poortmans et al.[65] fabricated a 4 terminal (4T) tandem architecture along with wide-band gap perovskites to study the influence on the V_{oc} of the device, focused on the perovskite/HTL interface. $MAPb(I_{0.6}Br_{0.4})_3$ and $Cs_{0.15}FA_{0.85}Pb(I_{0.71}Br_{0.29})_3$ perovskites with band gaps of 1.77 and 1.72 eV, respectively, were investigated.

It was shown that by surface passivation layer of Al_2O_3 it is possible to increase the V_{oc} of the perovskite solar cell without any correlation to the type of the HTL, as reflected from the graph in Figure 10A. Therefore, the V_{oc} is not fully dependent on the ionization potential of the HTL but also on the quality of the perovskite/HTL interface. The V_{oc} enhancement, which can be seen from the $J-V$ curve in Figure 10B, is mainly due to reduced nonradiative recombination of charge carriers through the passivation of dangling bonds at the surface. Passivated CsFAPbIBr demonstrated PCE of 27.1% in the 4T CsFAPbIBr-Si tandem solar cell.

> Thin films usually suffer from spectral losses due to insufficient light absorption. A possible way to overcome this limitation is by partial coverage of the surface by perovskite in order to form a semitransparent substance.

An additional option to fabricate the 4T tandem configuration is by using two perovskites solar cells with different band gaps (i.e., bottom cell and top cell). In this case, the top cell will have a wide band gap and the bottom cell will have a low band gap perovskite.

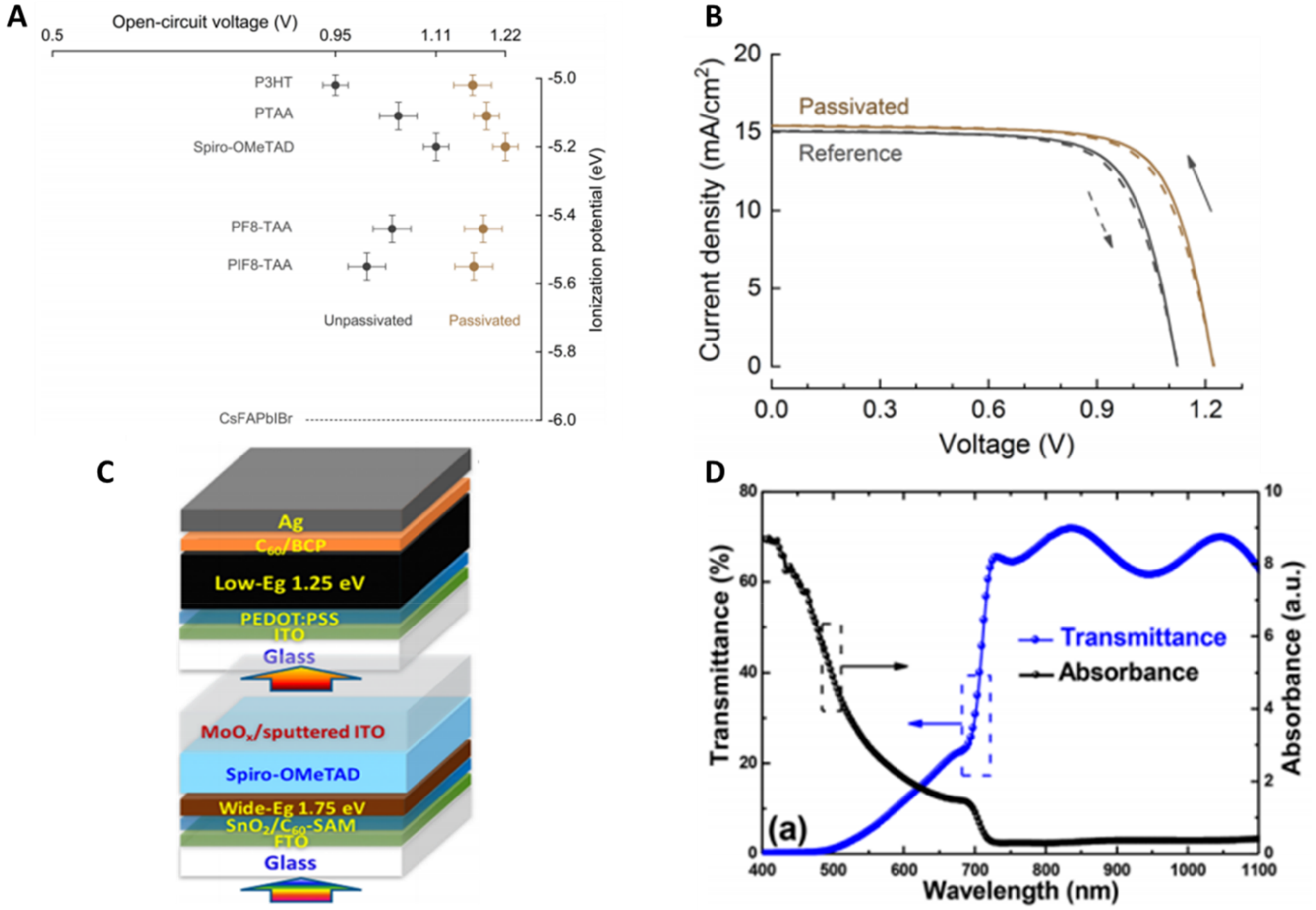

Figure 10. (a) Difference in the open-circuit voltage for several HTMs with (brown) and without (black) the Al_2O_3 passivation layer. (b) *J*–*V* curves of passivated and nonpassivated solar cells. (c) Schematic illustration of the 4T all-perovskite solar cell. (d) Absorption and transmittance spectra of the 1.75 eV perovskite top cell. Reprinted with permission from refs 65 and 66. Copyright 2019 and 2018 American Chemical Society.

Yan et al. demonstrated a 4T tandem based solely on perovskite.[66] They used $Cs_{0.2}FA_{0.8}Pb(I_{0.7}Br_{0.3})_3$ for the top cell (E_g = 1.75 eV) and $(FASnI_3)_{0.6}(MAPbI_3)_{0.4}$ composition for the bottom cell (E_g = 1.25 eV) along with a transparent MoO_x/ITO electrode, as can be seen in the schematic illustration in Figure 10C. Two main strategies were used to improve the efficiency of the 4T perovskite tandem solar cell. The first was widening the band gap of the top cell, which allows more light in the NIR region to pass through which then can be absorbed at the bottom cell (Figure 10D). In addition, a fabrication of a transparent electrode which demonstrated 70% AVT in the region above 700 nm wavelength reduced the spectral losses and enhanced the light absorption in the absorber's layers. Overall, this 4T all-perovskite tandem configuration demonstrated a PCE of 23.1%. This was the first time that an all-perovskite tandem solar cell exceeded the PCE of a world record single-junction perovskite solar cell.

Another kind of tandem configuration is 2T solar cells. In this case, there is a need to create an interconnecting layer (recombination layer) that should be conductive and transparent in order to allow light absorption at the bottom cell. Song et al.[67] used the same perovskites as described above in a 2T configuration with an interconnecting layer of Ag/MoO_3/ITO which provides optical and electrical connection and protects the layers underneath. The optical and electronic properties of the interconnecting layer can be tuned according to the perovskites type by changing the materials or the thickness of each layer. The 2T all-perovskite configuration showed a PCE of 21% and high stability for 100 h.

Photovoltaic technology has developed in recent years because of the ever-growing demand for greener and cleaner energy sources. The remarkable progress in perovskite-based solar cells has opened the way for a variety of deposition and fabrication techniques. The easy and low-cost fabrication process of perovskite materials, along with the possibility to achieve high power conversion efficiency, makes them an attractive solution for renewable energy. One of the exciting properties of perovskite is the ability to make it semitransparent and therefore to fabricate a semitransparent perovskite solar cell that potentially can be integrated into buildings as windows, for example.

However, one of the main remaining challenges in the field is the scale-up process of solar cells, where the goal is to fabricate a semitransparent solar cell that can be used instead of a window. Therefore, the perovskite deposition method should be suitable for large-scale devices. To date, the most common deposition technique is the spin-coating process, where a uniform thin film of perovskite can be produced. However, this process is suitable only for small devices at lab-scale. Other options such as inkjet printing, screen printing, evaporation, and slot die coating are possible alternatives for large-scale cells.

Moreover, thin films usually suffer from spectral losses due to insufficient light absorption. A possible way to overcome this limitation is by partial coverage of the surface by perovskite in order to form a semitransparent substance. To this end, the dewetting and self-assembly methods are used. Here, there are no spectral losses; however, the coverage is incomplete. In addition, with self-assembly, the deposition is made by a screen-printing technique that is suitable for large areas.

In looking ahead, there are several issues that need to be addressed: (i) sealing the empty (transparent) areas at the substrate to prevent enhanced recombination between the ETL and the HTM. A possible way to achieve this is by using a transparent nonconductive material that can be integrated selectively into the empty areas in the active area; (ii) finding a way in which the semitransparent devices can be stable under rough environmental conditions; (iii) the physical limit of these semitransparent devices where increasing the transparency will decrease the efficiency, which represents the main challenge. For the semitransparent perovskite solar cells to be a competitive technology, they must be brought to a point where the transparency can be controlled and the efficiency is maximized with each transparency. The development of semitransparent perovskite cells not only contributes to the building-integrated PV (BIPV) technology but also advances the tandem solar cell configuration where perovskite and Si or CIGS technologies are combined.

For the semitransparent perovskite solar cells to be a competitive technology, they must be brought to a point where the transparency can be controlled and the efficiency is maximized with each transparency.

The need for semitransparent solar cells is growing, because it can open the possibility to generating clean energy without sacrificing more open areas. Therefore, harnessing the potential of perovskite in this important field of semitransparent cells is necessary. Because of its attractive properties, perovskite can open the possibility of fabricating semitransparent solar cells with high efficiency and at low cost.

■ AUTHOR INFORMATION

Corresponding Author

Liioz Etgar – *Institute of Chemistry, Casali Center for Applied Chemistry, The Hebrew University of Jerusalem, Jerusalem 91904, Israel;* orcid.org/0000-0001-6158-8520; Email: lioz.etgar@mail.huji.ac.il

Author

Stav Rahmany – *Institute of Chemistry, Casali Center for Applied Chemistry, The Hebrew University of Jerusalem, Jerusalem 91904, Israel*

Complete contact information is available at: https://pubs.acs.org/10.1021/acsenergylett.0c00417

Notes

The authors declare no competing financial interest.

Biographies

Stav Rahmany is a Ph.D. student in Prof. Lioz Etgar's research group from the Institute of Chemistry at the Hebrew University of Jerusalem. Stav's research is focused on perovskite solar cell structure, including fabrication of semitransparent devices. He received his B.Sc in chemistry and biology and M.Sc in materials chemistry from the Hebrew University of Jerusalem.

Prof. Etgar is an Associate Professor at the Hebrew University of Jerusalem. He was the first to demonstrate the possibility of working with the perovskite as a light harvester and hole conductor in solar cells. Prof. Etgar is researching new semiconductor materials while designing and controlling their structure and properties to improve the photovoltaic parameters.

■ ACKNOWLEDGMENTS

This work was supported by the Israel Science Foundation Grant No. 937/18, the Israel Ministry of Science and the Singapore Reseach Foundation under CREATE: NTU:HUJI nanomaterials for energy and energy–water nexus program.

■ REFERENCES

(1) NREL. Best Research-Cell Efficiency Chart | Photovoltaic Research | NREL. https://www.nrel.gov/pv/cell-efficiency.html (accessed 2020-02-10).

(2) Li, C.; Lu, X.; Ding, W.; Feng, L.; Gao, Y.; Guo, Z. Formability of ABX 3 (X = F, Cl, Br, I) Halide Perovskites. *Acta Crystallogr., Sect. B: Struct. Sci.* **2008**, *64* (6), 702–707.

(3) Eperon, G. E.; Stranks, S. D.; Menelaou, C.; Johnston, M. B.; Herz, L. M.; Snaith, H. J. Formamidinium Lead Trihalide: A Broadly Tunable Perovskite for Efficient Planar Heterojunction Solar Cells. *Energy Environ. Sci.* **2014**, *7* (3), 982.

(4) Ono, L. K.; Juarez-Perez, E. J.; Qi, Y. Progress on Perovskite Materials and Solar Cells with Mixed Cations and Halide Anions. *ACS Appl. Mater. Interfaces* **2017**, *9*, 30197–30246.

(5) Saliba, M.; Matsui, T.; Seo, J. Y.; Domanski, K.; Correa-Baena, J. P.; Nazeeruddin, M. K.; Zakeeruddin, S. M.; Tress, W.; Abate, A.; Hagfeldt, A.; et al. Cesium-Containing Triple Cation Perovskite Solar Cells: Improved Stability, Reproducibility and High Efficiency. *Energy Environ. Sci.* **2016**, *9* (6), 1989–1997.

(6) Pellet, N.; Gao, P.; Gregori, G.; Yang, T.-Y.; Nazeeruddin, M. K.; Maier, J.; Grätzel, M. Mixed-Organic-Cation Perovskite Photovoltaics for Enhanced Solar-Light Harvesting. *Angew. Chem., Int. Ed.* **2014**, *53* (12), 3151–3157.

(7) Park, N. G. Perovskite Solar Cells: An Emerging Photovoltaic Technology. *Materials Today* **2015**, 65–72, DOI: 10.1016/j.mattod.2014.07.007.

(8) De Wolf, S.; Holovsky, J.; Moon, S. J.; Löper, P.; Niesen, B.; Ledinsky, M.; Haug, F. J.; Yum, J. H.; Ballif, C. Organometallic Halide Perovskites: Sharp Optical Absorption Edge and Its Relation to Photovoltaic Performance. *J. Phys. Chem. Lett.* **2014**, *5* (6), 1035–1039.

(9) Stranks, S. D.; Eperon, G. E.; Grancini, G.; Menelaou, C.; Alcocer, M. J. P.; Leijtens, T.; Herz, L. M.; Petrozza, A.; Snaith, H. J. Electron-Hole Diffusion Lengths Exceeding 1 Micrometer in an Organometal Trihalide Perovskite Absorber. *Science (Washington, DC, U. S.)* **2013**, *342* (6156), 341–344.

(10) Zhumekenov, A. A.; Saidaminov, M. I.; Haque, M. A.; Alarousu, E.; Sarmah, S. P.; Murali, B.; Dursun, I.; Miao, X. H.; Abdelhady, A. L.; Wu, T.; et al. Formamidinium Lead Halide Perovskite Crystals with Unprecedented Long Carrier Dynamics and Diffusion Length. *ACS Energy Lett.* **2016**, *1* (1), 32–37.

(11) Chang, Y. H.; Park, C. H.; Matsuishi, K. First-Principles Study of the Structural and the Electronic Properties of the Lead-Halide. *J. Korean Phys. Soc.* **2004**, *44* (4), 889–893.

(12) Kulkarni, S. A.; Baikie, T.; Boix, P. P.; Yantara, N.; Mathews, N.; Mhaisalkar, S. Band-Gap Tuning of Lead Halide Perovskites

Using a Sequential Deposition Process. *J. Mater. Chem. A* **2014**, *2* (24), 9221−9225.

(13) Liu, M.; Johnston, M. B.; Snaith, H. J. Efficient Planar Heterojunction Perovskite Solar Cells by Vapour Deposition. *Nature* **2013**, *501* (7467), 395−398.

(14) Burschka, J.; Pellet, N.; Moon, S. J.; Humphry-Baker, R.; Gao, P.; Nazeeruddin, M. K.; Grätzel, M. Sequential Deposition as a Route to High-Performance Perovskite-Sensitized Solar Cells. *Nature* **2013**, *499* (7458), 316−319.

(15) Chen, C.-W.; Kang, H.-W.; Hsiao, S.-Y.; Yang, P.-F.; Chiang, K.-M.; Lin, H.-W. Efficient and Uniform Planar-Type Perovskite Solar Cells by Simple Sequential Vacuum Deposition. *Adv. Mater.* **2014**, *26* (38), 6647−6652.

(16) Schneider, A.; Alon, S.; Etgar, L. Evolution of Photovoltaic Performance in Fully Printable Mesoscopic Carbon-Based Perovskite Solar Cells. *Energy Technol.* **2019**, *7* (7), 1900481.

(17) Energy Information Administration. *Residential Energy Consumption Survey (RECS)*; https://www.eia.gov/consumption/residential/index.php (accessed 2020-02-11).

(18) U.S. DOE. *Energy Information Administration, Commercial Buildings Energy Consumption Survey*; 2003.

(19) Walsh, A. Principles of Chemical Bonding and Band Gap Engineering in Hybrid Organic-Inorganic Halide Perovskites. *J. Phys. Chem. C* **2015**, *119* (11), 5755−5760.

(20) Yuan, L.; Wang, Z.; Duan, R.; Huang, P.; Zhang, K.; Chen, Q.; Allam, N. K.; Zhou, Y.; Song, B.; Li, Y. Semi-Transparent Perovskite Solar Cells: Unveiling the Trade-off between Transparency and Efficiency. *J. Mater. Chem. A* **2018**, *6* (40), 19696−19702.

(21) Yang, Z.; Chueh, C. C.; Liang, P. W.; Crump, M.; Lin, F.; Zhu, Z.; Jen, A. K. Y. Effects of Formamidinium and Bromide Ion Substitution in Methylammonium Lead Triiodide toward High-Performance Perovskite Solar Cells. *Nano Energy* **2016**, *22*, 328−337.

(22) Ball, J. M.; Stranks, S. D.; Hörantner, M. T.; Hüttner, S.; Zhang, W.; Crossland, E. J. W.; Ramirez, I.; Riede, M.; Johnston, M. B.; Friend, R. H.; et al. Optical Properties and Limiting Photocurrent of Thin-Film Perovskite Solar Cells. *Energy Environ. Sci.* **2015**, *8* (2), 602−609.

(23) Chen, W.; Zhang, J.; Xu, G.; Xue, R.; Li, Y.; Zhou, Y.; Hou, J.; Li, Y. A Semitransparent Inorganic Perovskite Film for Overcoming Ultraviolet Light Instability of Organic Solar Cells and Achieving 14.03% Efficiency. *Adv. Mater.* **2018**, *30* (21), 1800855.

(24) Liu, C.; Li, W.; Zhang, C.; Ma, Y.; Fan, J.; Mai, Y. All-Inorganic CsPbI2Br Perovskite Solar Cells with High Efficiency Exceeding 13%. *J. Am. Chem. Soc.* **2018**, *140* (11), 3825−3828.

(25) Kim, H. S.; Park, N. G. Parameters Affecting I-V Hysteresis of CH3NH3PbI3 Perovskite Solar Cells: Effects of Perovskite Crystal Size and Mesoporous TiO2 Layer. *J. Phys. Chem. Lett.* **2014**, *5* (17), 2927−2934.

(26) Bag, S.; Durstock, M. F. Efficient Semi-Transparent Planar Perovskite Solar Cells Using a 'Molecular Glue.'. *Nano Energy* **2016**, *30*, 542−548.

(27) Kim, H. B.; Choi, H.; Jeong, J.; Kim, S.; Walker, B.; Song, S.; Kim, J. Y. Mixed Solvents for the Optimization of Morphology in Solution-Processed, Inverted-Type Perovskite/Fullerene Hybrid Solar Cells. *Nanoscale* **2014**, *6* (12), 6679−6683.

(28) Cao, X.; Zhi, L.; Jia, Y.; Li, Y.; Zhao, K.; Cui, X.; Ci, L.; Zhuang, D.; Wei, J. A Review of the Role of Solvents in Formation of High-Quality Solution-Processed Perovskite Films. *ACS Appl. Mater. Interfaces* **2019**, 7639−7654, DOI: 10.1021/acsami.8b16315.

(29) Ponchai, J.; Kaewurai, P.; Boonthum, C.; Pinsuwan, K.; Supasai, T.; Sahasithiwat, S.; Kanjanaboos, P. Modifying Morphology and Defects of Low-Dimensional, Semi-Transparent Perovskite Thin Films: Via Solvent Type. *RSC Adv.* **2019**, *9* (21), 12047−12054.

(30) Magdassi, S.; Grouchko, M.; Toker, D.; Kamyshny, A.; Balberg, I.; Millo, O. Ring Stain Effect at Room Temperature in Silver Nanoparticles Yields High Electrical Conductivity. *Langmuir* **2005**, *21* (23), 10264−10267.

(31) Misra, R. K.; Aharon, S.; Layani, M.; Magdassi, S.; Etgar, L. A Mesoporous-Planar Hybrid Architecture of Methylammonium Lead Iodide Perovskite Based Solar Cells. *J. Mater. Chem. A* **2016**, *4* (37), 14423−14429.

(32) Aharon, S.; Layani, M.; Cohen, B. El; Shukrun, E.; Magdassi, S.; Etgar, L. Self-Assembly of Perovskite for Fabrication of Semi-transparent Perovskite Solar Cells. *Adv. Mater. Interfaces* **2015**, *2* (12), 1500118.

(33) Roldán-Carmona, C.; Malinkiewicz, O.; Betancur, R.; Longo, G.; Momblona, C.; Jaramillo, F.; Camacho, L.; Bolink, H. J. High Efficiency Single-Junction Semitransparent Perovskite Solar Cells. *Energy Environ. Sci.* **2014**, *7* (9), 2968−2973.

(34) Kim, G. M.; Tatsuma, T. Semitransparent Solar Cells with Ultrasmooth and Low-Scattering Perovskite Thin Films. *J. Phys. Chem. C* **2016**, *120* (51), 28933−28938.

(35) Rahmany, S.; Layani, M.; Magdassi, S.; Etgar, L. Fully Functional Semi-Transparent Perovskite Solar Cell Fabricated in Ambient Air. *Sustain. Energy Fuels* **2017**, *1* (10), 2120−2127.

(36) Solanki, A.; Yadav, P.; Turren-Cruz, S. H.; Lim, S. S.; Saliba, M.; Sum, T. C. Cation Influence on Carrier Dynamics in Perovskite Solar Cells. *Nano Energy* **2019**, *58*, 604−611.

(37) Saliba, M.; Matsui, T.; Seo, J. Y.; Domanski, K.; Correa-Baena, J. P.; Nazeeruddin, M. K.; Zakeeruddin, S. M.; Tress, W.; Abate, A.; Hagfeldt, A.; et al. Cesium-Containing Triple Cation Perovskite Solar Cells: Improved Stability, Reproducibility and High Efficiency. *Energy Environ. Sci.* **2016**, *9* (6), 1989−1997.

(38) Lee, J. W.; Kim, D. H.; Kim, H. S.; Seo, S. W.; Cho, S. M.; Park, N. G. Formamidinium and Cesium Hybridization for Photo- and Moisture-Stable Perovskite Solar Cell. *Adv. Energy Mater.* **2015**, *5* (20), 1501310.

(39) Rai, M.; Rahmany, S.; Lim, S. S.; Magdassi, S.; Wong, L. H.; Etgar, L. Hot Dipping Post Treatment for Improved Efficiency in Micro Patterned Semi-Transparent Perovskite Solar Cells. *J. Mater. Chem. A* **2018**, *6* (46), 23787−23796.

(40) Lee, W.; Lee, J.; Yun, H.; Kim, J.; Park, J.; Choi, C.; Kim, D. C.; Seo, H.; Lee, H.; Yu, J. W.; et al. High-Resolution Spin-on-Patterning of Perovskite Thin Films for a Multiplexed Image Sensor Array. *Adv. Mater.* **2017**, *29* (40), 1702902.

(41) Beckel, D.; Dubach, A.; Grundy, A. N.; Infortuna, A.; Gauckler, L. J. Solid-State Dewetting of La0.6Sr0.4Co0.2Fe0.8O3$\pm\delta$ Thin Films during Annealing. *J. Eur. Ceram. Soc.* **2008**, *28* (1), 49−60.

(42) Eperon, G. E.; Bryant, D.; Troughton, J.; Stranks, S. D.; Johnston, M. B.; Watson, T.; Worsley, D. A.; Snaith, H. J. Efficient, Semitransparent Neutral-Colored Solar Cells Based on Microstructured Formamidinium Lead Trihalide Perovskite. *J. Phys. Chem. Lett.* **2015**, *6* (1), 129−138.

(43) Eperon, G. E.; Burlakov, V. M.; Goriely, A.; Snaith, H. J. Neutral Color Semitransparent Microstructured Perovskite Solar Cells. *ACS Nano* **2014**, *8* (1), 591−598.

(44) Chen, S.; Chen, B.; Gao, X.; Dong, B.; Hu, H.; Yan, K.; Wen, W.; Zou, D. Neutral-Colored Semitransparent Solar Cells Based on Pseudohalide (SCN-)-Doped Perovskite. *Sustain. Energy Fuels* **2017**, *1* (5), 1034−1040.

(45) Gheno, A.; Vedraine, S.; Ratier, B.; Bouclé, J. π-Conjugated Materials as the Hole-Transporting Layer in Perovskite Solar Cells. *Metals* **2016**, 21 DOI: 10.3390/met6010021.

(46) Safari, Z.; Zarandi, M. B.; Giuri, A.; Bisconti, F.; Carallo, S.; Listorti, A.; Corcione, C. E.; Nateghi, M. R.; Rizzo, A.; Colella, S. Optimizing the Interface between Hole Transporting Material and Nanocomposite for Highly Efficient Perovskite Solar Cells. *Nanomaterials* **2019**, *9* (11), 1627.

(47) Singh, R.; Singh, P. K.; Bhattacharya, B.; Rhee, H. W. Review of Current Progress in Inorganic Hole-Transport Materials for Perovskite Solar Cells. *Applied Materials Today* **2019**, 175−200, DOI: 10.1016/j.apmt.2018.12.011.

(48) Prochowicz, D.; Tavakoli, M. M.; Wolska-Pietkiewicz, M.; Jędrzejewska, M.; Trivedi, S.; Kumar, M.; Zakeeruddin, S. M.; Lewiński, J.; Graetzel, M.; Yadav, P. Suppressing Recombination in Perovskite Solar Cells via Surface Engineering of TiO2 ETL. *Sol. Energy* **2020**, *197*, 50−57.

(49) Chen, J.; Park, N. G. Causes and Solutions of Recombination in Perovskite Solar Cells. *Adv. Mater.* **2019**, 1803019 DOI: 10.1002/adma.201803019.

(50) Heo, J. H.; Jang, M. H.; Lee, M. H.; Han, H. J.; Kang, M. G.; Lee, M. L.; Im, S. H. Efficiency Enhancement of Semi-Transparent Sandwich Type $CH_3NH_3PbI_3$ Perovskite Solar Cells with Island Morphology Perovskite Film by Introduction of Polystyrene Passivation Layer. *J. Mater. Chem. A* **2016**, *4* (42), 16324−16329.

(51) Zhang, L.; Hörantner, M. T.; Zhang, W.; Yan, Q.; Snaith, H. J. Near-Neutral-Colored Semitransparent Perovskite Films Using a Combination of Colloidal Self-Assembly and Plasma Etching. *Sol. Energy Mater. Sol. Cells* **2017**, *160*, 193−202.

(52) Lang, F.; Gluba, M. A.; Albrecht, S.; Rappich, J.; Korte, L.; Rech, B.; Nickel, N. H. Perovskite Solar Cells with Large-Area CVD-Graphene for Tandem Solar Cells. *J. Phys. Chem. Lett.* **2015**, *6* (14), 2745−2750.

(53) Morales-Masis, M.; De Wolf, S.; Woods-Robinson, R.; Ager, J. W.; Ballif, C. Transparent Electrodes for Efficient Optoelectronics. *Adv. Electron. Mater.* **2017**, *3* (5), 1600529.

(54) Della Gaspera, E.; Peng, Y.; Hou, Q.; Spiccia, L.; Bach, U.; Jasieniak, J. J.; Cheng, Y. B. Ultra-Thin High Efficiency Semi-transparent Perovskite Solar Cells. *Nano Energy* **2015**, *13*, 249−257.

(55) Dou, B.; Miller, E. M.; Christians, J. A.; Sanehira, E. M.; Klein, T. R.; Barnes, F. S.; Shaheen, S. E.; Garner, S. M.; Ghosh, S.; Mallick, A.; et al. High-Performance Flexible Perovskite Solar Cells on Ultrathin Glass: Implications of the TCO. *J. Phys. Chem. Lett.* **2017**, *8* (19), 4960−4966.

(56) Werner, J.; Dubuis, G.; Walter, A.; Löper, P.; Moon, S. J.; Nicolay, S.; Morales-Masis, M.; De Wolf, S.; Niesen, B.; Ballif, C. Sputtered Rear Electrode with Broadband Transparency for Perovskite Solar Cells. *Sol. Energy Mater. Sol. Cells* **2015**, *141*, 407−413.

(57) Chang, C. Y.; Lee, K. T.; Huang, W. K.; Siao, H. Y.; Chang, Y. C. High-Performance, Air-Stable, Low-Temperature Processed Semi-transparent Perovskite Solar Cells Enabled by Atomic Layer Deposition. *Chem. Mater.* **2015**, *27* (14), 5122−5130.

(58) Bush, K. A.; Bailie, C. D.; Chen, Y.; Bowring, A. R.; Wang, W.; Ma, W.; Leijtens, T.; Moghadam, F.; McGehee, M. D. Thermal and Environmental Stability of Semi-Transparent Perovskite Solar Cells for Tandems Enabled by a Solution-Processed Nanoparticle Buffer Layer and Sputtered ITO Electrode. *Adv. Mater.* **2016**, *28* (20), 3937−3943.

(59) Werner, J.; Geissbühler, J.; Dabirian, A.; Nicolay, S.; Morales-Masis, M.; Wolf, S. De; Niesen, B.; Ballif, C. Parasitic Absorption Reduction in Metal Oxide-Based Transparent Electrodes: Application in Perovskite Solar Cells. *ACS Appl. Mater. Interfaces* **2016**, *8* (27), 17260−17267.

(60) Raiford, J. A.; Belisle, R. A.; Bush, K. A.; Prasanna, R.; Palmstrom, A. F.; McGehee, M. D.; Bent, S. F. Atomic Layer Deposition of Vanadium Oxide to Reduce Parasitic Absorption and Improve Stability in N-i-p Perovskite Solar Cells for Tandems. *Sustain. Energy Fuels* **2019**, *3* (6), 1517−1525.

(61) Noh, Y. J.; Kim, J. G.; Kim, S. S.; Kim, H. K.; Na, S. I. Efficient Semi-Transparent Perovskite Solar Cells with a Novel Indium Zinc Tin Oxide Top Electrode Grown by Linear Facing Target Sputtering. *J. Power Sources* **2019**, *437*, 226894.

(62) Han, K.; Xie, M.; Zhang, L.; Yan, L.; Wei, J.; Ji, G.; Luo, Q.; Lin, J.; Hao, Y.; Ma, C. Q. Fully Solution Processed Semi-Transparent Perovskite Solar Cells with Spray-Coated Silver Nanowires/ZnO Composite Top Electrode. *Sol. Energy Mater. Sol. Cells* **2018**, *185*, 399−405.

(63) Lu, H.; Lin, J.; Wu, N.; Nie, S.; Luo, Q.; Ma, C. Q.; Cui, Z. Inkjet Printed Silver Nanowire Network as Top Electrode for Semi-Transparent Organic Photovoltaic Devices. *Appl. Phys. Lett.* **2015**, *106* (9), 093302.

(64) Kim, K. M.; Ahn, S.; Jang, W.; Park, S.; Park, O. O.; Wang, D. H. Work Function Optimization of Vacuum Free Top-Electrode by PEDOT:PSS/PEI Interaction for Efficient Semi-Transparent Perovskite Solar Cells. *Sol. Energy Mater. Sol. Cells* **2018**, *176*, 435−440.

(65) Jaysankar, M.; Raul, B. A. L.; Bastos, J.; Burgess, C.; Weijtens, C.; Creatore, M.; Aernouts, T.; Kuang, Y.; Gehlhaar, R.; Hadipour, A.; et al. Minimizing Voltage Loss in Wide-Bandgap Perovskites for Tandem Solar Cells. *ACS Energy Lett.* **2019**, *4* (1), 259−264.

(66) Zhao, D.; Wang, C.; Song, Z.; Yu, Y.; Chen, C.; Zhao, X.; Zhu, K.; Yan, Y. Four-Terminal All-Perovskite Tandem Solar Cells Achieving Power Conversion Efficiencies Exceeding 23%. *ACS Energy Lett.* **2018**, *3* (2), 305−306.

(67) Zhao, D.; Chen, C.; Wang, C.; Junda, M. M.; Song, Z.; Grice, C. R.; Yu, Y.; Li, C.; Subedi, B.; Podraza, N. J.; et al. Efficient Two-Terminal All-Perovskite Tandem Solar Cells Enabled by High-Quality Low-Bandgap Absorber Layers. *Nat. Energy* **2018**, *3* (12), 1093−1100.